

Estimation of Output Voltage Ripple in Phase-Staggered Series-Connected Two-Quadrant Power Converters for Electromagnets in Particle Accelerators

Research paper

Pokharkar Rahul Rohidas^{1,2,*}, Mangesh Borage^{1,2}, Alok Singh¹, Vineet Kumar Dwivedi¹, Abhishek Srivastava¹

¹Raja Ramanna Centre for Advanced Technology, Indore 452013, India

²Homi Bhabha National Institute, Mumbai 400094, India

Received: 13, April 2023; Accepted: 01, June 2023

Abstract: In booster synchrotron, fast-ramped power converters (FRPCs) are used for ramping up the magnetic field of electromagnets connected in series, at a fast rate, typically 1,000s of ampere per second. In large accelerators, the number of electromagnets is large. Therefore, during ramping, the peak value of driving voltage becomes prohibitively large considering the insulation requirement of the magnets and cables. The power converter is therefore developed by connecting a suitable number of smaller voltage rated modules in series. The series-connected modules are operated in phase-staggered mode to reduce the output voltage ripple or to reduce the filtering requirement to meet the prescribed ripple voltage. Since the filter component values predominantly decide the dynamic response, the achievable small-signal bandwidth of the control loop and hence the achievable tracking accuracy of the ramping output current are essentially governed by the filter components. To optimise the filter design, quantification of overall ripple voltage is crucial, that too under the most practical conditions considering non-ideal conditions. In this paper, estimation of overall ripple voltage is performed for series-connected two-quadrant power converters (TQPCs) operating in phase-staggering mode for ideal and non-ideal conditions. Simulation and experimental verification results are shown to be in good agreement with the analytical results.

Keywords: fast-ramped power converter • two-quadrant power converter • series-connected power converters

1. Introduction

The particle accelerator is a machine that is used for accelerating the beam of charged particles to very high energy. It is a machine of utmost importance from the point of view of researchers in the fields of nuclear physics, material science, and medical and industrial applications (Barbalat, 1992; Chao and Chou, 2011; Visintini, 2014). In particle accelerators, electromagnets are used for various purposes such as bending, focussing, defocussing, and correction of chromaticity, as well as to control Landau damping. Power converters are used to energise electromagnets. When current is flown through the coil of an electromagnet, a magnetic field is produced. The quality of this magnetic field is dependent on the current flowing through the magnet coil (Burnet, 2014).

Electromagnets can be energised either individually or by connecting electromagnets in series. Individual connection provides flexibility in setting the magnetic field in each magnet. However, it is difficult to maintain an

* Email: rahulpokharkar@rrcat.gov.in

identical magnetic field waveform in each magnet. On the other hand, series connection of electromagnets facilitates maintaining the same magnetic field in each magnet. In booster synchrotron, there is requirement of the same magnetic field waveform in each magnet. Thus, series connection is a preferred option for energising magnets of booster synchrotrons (Burnet, 2014). In large accelerators, the number of magnets to be energised in series is large in number. The peak voltage encountered by the power converter is prohibitively large during ramping. To minimise this voltage such that it is contained within feasible limits, the total number of magnets are divided into a number of smaller sections of magnets in series and each section of magnets is energised by a separate power converter. The power converter, depending on the power levels involved, may itself need to be developed not as a single unit but by connecting suitably rated modules in series and/or parallel (Gros et al., 2006; Pont et al., 2010; Shimogawa et al., 2019; Visintini et al., 2008).

In booster synchrotron, fast-ramped power converters (FRPC) are used for ramping up a magnetic field at a fast rate (typically within 100s of milliseconds) in synchronism with energy of charged particle (Bouteille, 2014; Burnet, 2014). The FRPC is either a switch-mode two-quadrant power converter (TQPC) or a four-quadrant power converter (FQPC). Output current should be ramped up and down as guided by the current reference waveform, precisely with the prescribed, stringent tracking accuracy. Tracking accuracy is a critical parameter in the designing of FRPCs in order to track the reference faithfully. Use of switch-mode power converters as FRPCs is increased with advent of high-power, high-speed power semiconductor devices (Gros et al., 2006; Marks et al., 2002; Rodrigues et al., 2019; Shimogawa et al., 2019; Visintini et al., 2008). Tracking accuracy is governed by the control-loop bandwidth (Srivastava et al., 2023). Filter component values decides the cutoff frequency, which in turn affects the bandwidth. Filter component values are governed by ripple voltage. As far as series-connected modular power converters are concerned, overall voltage ripple is reduced with the phase-staggering operation under optimum phase shift. This results in reduction in filter component values, which increases the control-loop bandwidth. This, in turn, improves the tracking accuracy. Thus, quantification of ripple voltage is crucial in ideal as well as the most practical conditions considering non-ideal conditions, such as filter component tolerances, unequal input DC voltages, unequal duty cycles, and unequal on-state voltage drops in semiconductor devices. The present study estimates the overall ripple voltage in series-connected TQPCs under ideal as well as non-ideal conditions.

The remaining part of the paper is organised as follows. Section 2 describes the series-connected TQPCs, wherein the equation of output voltage of an individual TQPC is derived. In Section 3, an analysis of 2-, 3-, 4-series-connected TQPCs is presented for an ideal case. This analysis is extrapolated to n -series-connected TQPCs to provide important results, such as optimum phase shift, for which the overall ripple voltage is minimum, and expressions for duty-cycle values, for which the overall ripple voltage is minimum and maximum. In Section 4, analysis of two series-connected TQPCs is performed under various non-ideal conditions such as filter component tolerances, unequal input DC voltage of TQPCs, unequal duty cycles, and unequal on-state voltage drops in semiconductor devices. In Section 5, simulation and experimental verification results are presented. In Section 6, the conclusions are provided in a summarised form.

2. Series-Connected TQPCs

The circuit diagram of n -series-connected TQPCs is shown in Figure 1. TQPC₁ to TQPC _{n} are connected in series and energise magnet load, which is represented by a series-connected resistance and inductance R_m and L_m , respectively. The series-connected TQPCs are considered to be operating under common duty-cycle control (Shi et al., 2011), although their operation can be suitably staggered in phase, as discussed subsequently. Each TQPC has two switches S_{Ai} and S_{Bi} , two diodes D_{Ai} and D_{Bi} , filter inductor L_i , and filter capacitor C_i , and is fed with input DC voltage V_{DCi} . Here and throughout this paper, $i=1,2,\dots,n$. Individual outputs of TQPCs are given by $v_i(t)$ and the total output voltage is denoted by $v_0(t)$. Each output voltage can be considered to be composed on average or DC value (denoted by V_i) and the AC component representing ripple (denoted by $\tilde{v}_i(t)$). Thus, $v_i(t)=V_i+\tilde{v}_i(t)$. Similarly, $v_0(t)=V_0+\tilde{v}_0(t)$. Let the peak-to-peak ripple voltage in the output voltage of each TQPC be ΔV_i , and let ΔV_o be the peak-to-peak ripple voltage in the overall output voltage. Let the peak-to-peak inductor current ripple of each TQPC be ΔI_{Li} . Under ideal conditions, each TQPC is identical in all respects. Thus, $V_{DCi}=V_{DC}$, $L_i=L$, and

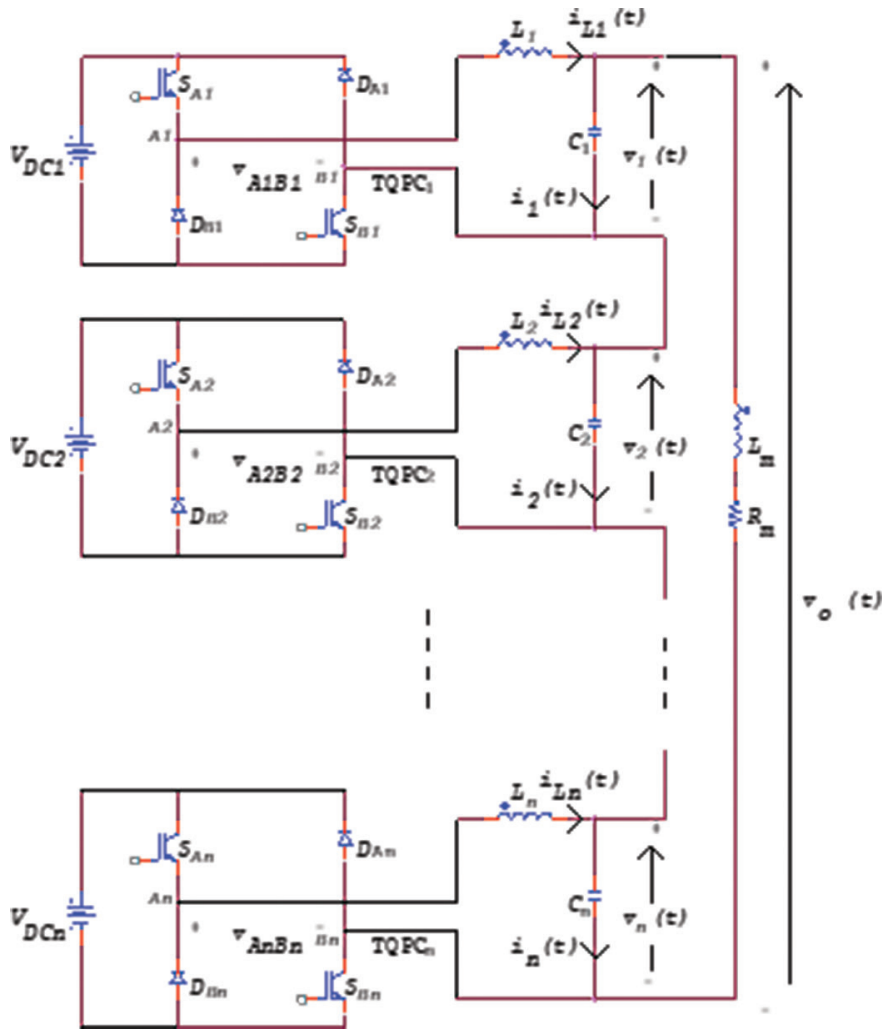


Fig. 1. Circuit diagram of series-connected TQPCs. TQPCs, two-quadrant power converters.

$C_i = C$. This results in $\Delta I_{Li} = \Delta I_L$ and $\Delta V_i = \Delta V$. The expressions for ΔI_L and ΔV can be derived as (Srivastava et al., 2021):

$$\Delta I_L = \begin{cases} \frac{V_{DC}(1-D)(2D-1)}{L} & \text{1st quadrant operation} \\ \frac{V_{DC}D(1-2D)}{L} & \text{2nd quadrant operation} \end{cases} \quad (1)$$

$$\Delta V = \frac{\Delta I_L}{16fC}$$

where f and D are the switching frequency and duty cycle of each TQPC.

Figure 2 shows the idealised steady-state waveforms of control signals of switches S_{A1} and S_{B1} (v_{g_A1} and v_{g_B1}), bridge output voltage (v_{AB1}), filter inductor current (i_{L1}), filter capacitor current (i_1), and output voltage (v_1) in the first quadrant operation of the TQPC (Srivastava, 2022). The figure also indicates various time periods used in the analysis presented in this paper. The time period of $\tilde{v}_1(t)$ is $\frac{T}{2}$, as the converter is working under a unipolar PWM control scheme, with T being the switching time period.

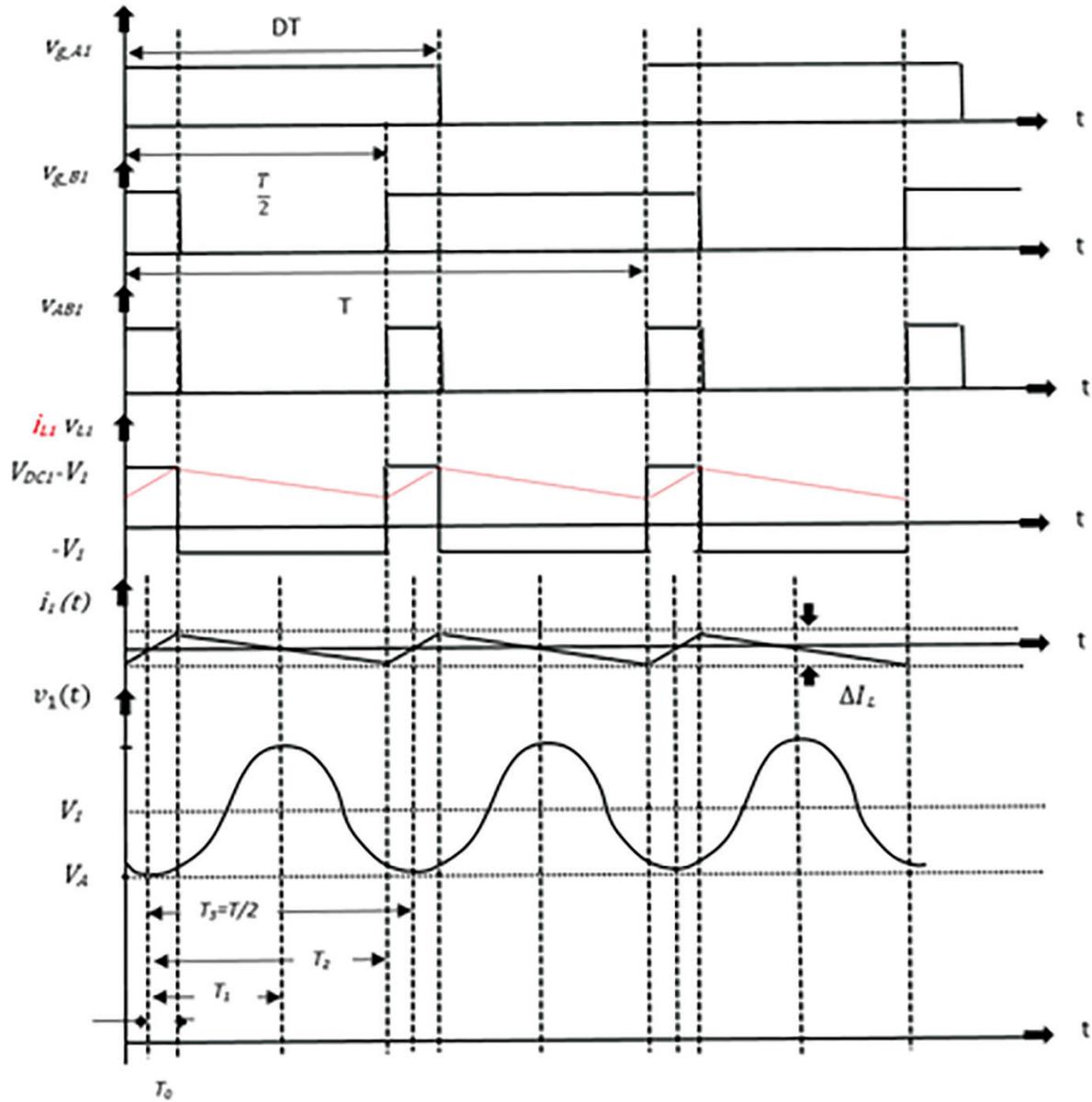


Fig. 2. Waveforms of 1st quadrant operation for TQPC1. TQPC, two-quadrant power converter.

The expression for $i_1(t)$ can be written as:

$$i_1(t) = \begin{cases} \frac{\Delta I_L t}{2T_0} & 0 \leq t < T_0 \\ \frac{-\Delta I_L}{2(T_1 - T_0)}(t - T_0) + \frac{\Delta I_L}{2} & T_0 \leq t < T_1 \\ \frac{-\Delta I_L}{2(T_2 - T_1)}(t - T_1) & T_1 \leq t < T_2 \\ \frac{\Delta I_L}{2(T_3 - T_2)}(t - T_2) - \frac{\Delta I_L}{2} & T_2 \leq t < T_3 \end{cases} \quad (2)$$

The expression for $v_1(t)$ can be derived as:

$$v_1(t) = \begin{cases} \frac{\Delta L_L t^2}{2CT_0} + V_A & 0 \leq t < T_0 \\ \frac{-\Delta L_L}{2C(T_1 - T_0)} \left(\frac{t^2}{2} - T_1 t - \frac{T_0^2}{2} + T_0 T_1 \right) + \frac{\Delta L_L T_0}{4C} + V_A & T_0 \leq t < T_1 \\ \frac{-\Delta L_L}{2C(T_2 - T_1)} \left(\frac{t^2}{2} - T_1 t - \frac{T_1^2}{2} \right) + V_A & T_1 \leq t < T_2 \\ \frac{\Delta L_L}{2C(T_3 - T_2)} \left(\frac{t^2}{2} - T_3 t - \frac{T_2^2}{2} + T_2 T_3 \right) - \frac{\Delta L_L (T_3 - T_2)}{4C} + V_A & T_2 \leq t < T_3 \end{cases} \quad (3)$$

where T_0, T_1, T_2 , and T_3 are given by:

$$T_0 = \frac{(D - 0.5)T}{2}, \quad T_1 = \frac{T}{4}, \quad T_2 = \frac{(3 - 2D)T}{4}, \quad T_3 = \frac{T}{2} \quad (4)$$

V_A is the initial value of the output voltage of TQPC as shown in Figure 2, and can be determined using Eq. (3) under the condition that the average value of $v_1(t)$ be equal to $V_1 = V_{DC1}(2D - 1)$. V_A is given by Eq. (5):

$$V_A = \frac{1}{T_3} \left[V_{DC1}(2D - 1) - \frac{\Delta L_L T_0^2}{6C} + \frac{\Delta L_L}{2C(T_1 - T_0)} \left(\frac{T_0^3}{3} - \frac{T_1^3}{3} + \frac{T_0 T_1^2}{2} - \frac{T_1 T_0^2}{2} \right) + \frac{\Delta L_L T_0 (T_0 - T_1)}{2C} \right. \\ \left. + \frac{\Delta L_L}{2C(T_2 - T_1)} \left(\frac{T_2^3}{6} - \frac{T_1 T_2^2}{2} - \frac{T_2 T_1^2}{2} + \frac{5T_1^3}{6} \right) + \frac{\Delta L_L}{2C(T_3 - T_2)} \left(\frac{T_3^3}{3} - \frac{T_2 T_3^2}{2} - \frac{T_3 T_2^2}{2} - \frac{T_2^2}{3} \right) \right. \\ \left. + \frac{\Delta L_L (T_3 - T_2)^2}{4C} \right] \quad (5)$$

3. Series-Connected Phase-Staggered TQPCs: Ideal Case

Phase-staggering in the operation of series-connected TQPCs can be introduced to reduce the ripple voltage in the overall output and to increase the ripple frequency, which can be carried out by introducing the suitable phase shift (Φ) in the control signals of switches in TQPC₂ to TQPC_n with respect to the control signals of TQPC₁. This phase shift, in turn, reflects by the same amount in the $v_2(t)$ to $v_n(t)$ (Yang et al., 2017). The effect of Φ on overall output voltage ripple in the series operation of TQPCs in ideal conditions is discussed in this section. To facilitate the analysis, the output voltage of TQPC₁ is first computed numerically using Eq. (3). Output voltages of TQPC₂ to TQPC_n are obtained by shifting the $\tilde{v}_1(t)$ in the time domain by an appropriate amount, which results in the required shift. $\tilde{v}_o(t)$ is obtained from the addition of $\tilde{v}_i(t)$. ΔV_o is obtained from the difference of maxima and minima of $\tilde{v}_o(t)$. The converter parameters given in Table 1 are considered for the analysis. The obtained waveforms of $\tilde{v}_i(t)$ and $\tilde{v}_o(t)$ for 2-, 3-, 4-series-connected phase-staggered TQPCs operating at $D = 0.6$ are illustrated in Figure 3.

Parameters	Value
V_{DC}	50 V
T	100 μ s
L	80 μ H
C	20 μ F

TQPCs, two-quadrant power converters.

Table 1. Parameters for analysis of series-connected TQPCs.

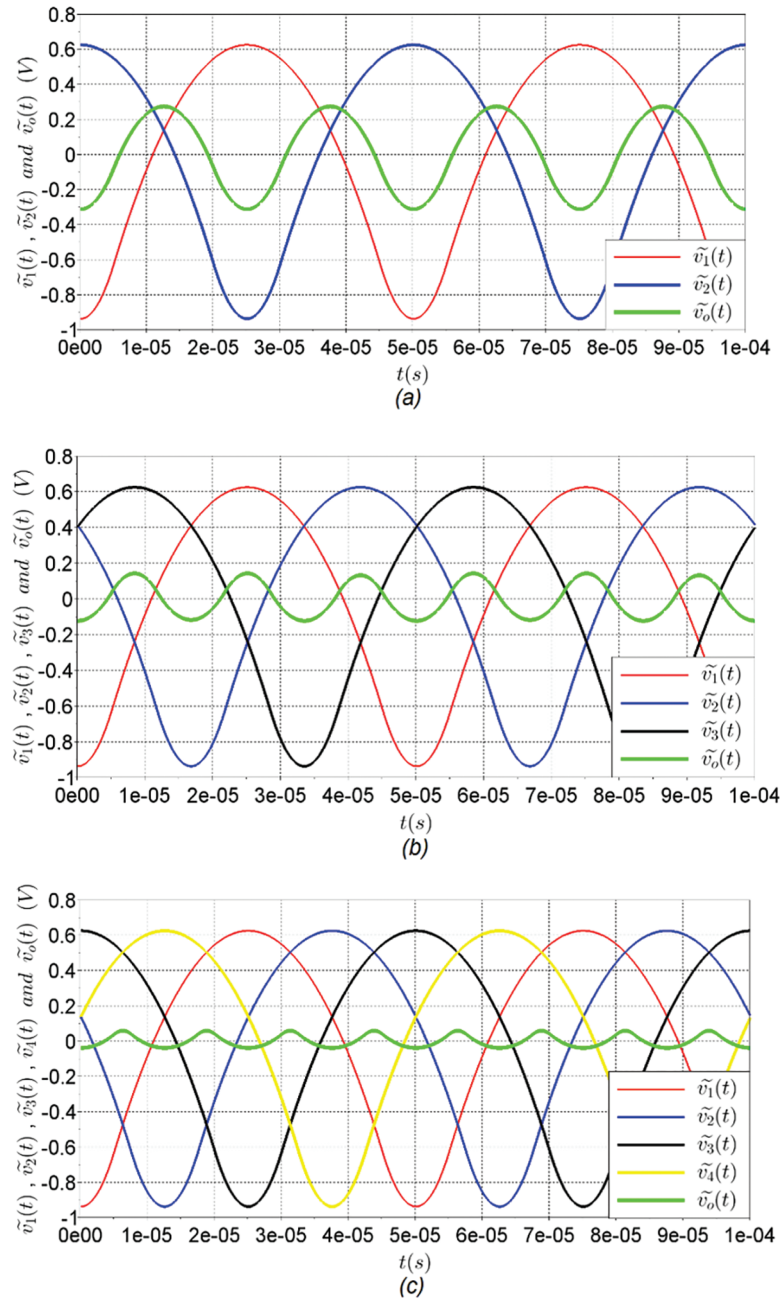


Fig. 3. Waveforms of $\tilde{v}_i(t)$ and $\tilde{v}_o(t)$ for (a) two TQPCs in series with $\Phi = \pi$ radians in control signals of TQPC₂ with respect to TQPC₁, (b) three TQPCs in series with $\Phi = 2\pi/3$ and $\Phi = 4\pi/3$ radians in control signals of TQPC₂ and TQPC₃, respectively, with respect to TQPC₁, and (c) four TQPCs in series with phase shift of $\Phi = \pi/2$, $\Phi = \pi$, and $\Phi = 3\pi/2$ radians in control signals of TQPC₂, TQPC₃ and TQPC₄, respectively, with respect to TQPC₁. TQPCs, two-quadrant power converters.

In each case, the waveform of $\tilde{v}_1(t)$ is obtained using Eq. (3). Subsequently, the waveforms of $\tilde{v}_i(t)$ are obtained by shifting the $\tilde{v}_1(t)$ in the time domain by an amount equivalent to the respective value of Φ . Then, $\tilde{v}_o(t)$ is obtained from the addition of $\tilde{v}_i(t)$. ΔV_o is obtained from the difference of maxima and minima of $\tilde{v}_o(t)$. The plot of variation of ΔV_o with Φ is depicted in Figure 4. It is observed from Figure 4 that ΔV_o is minimum for certain Φ , called the optimum phase shift (Φ_{opt}). The results are extrapolated to the operation of n TQPCs in series. Table 2 summarises the values of required phase shift resulting in minimum ΔV_o . In addition to reduction in ΔV_o , it is inferred from Figure 3

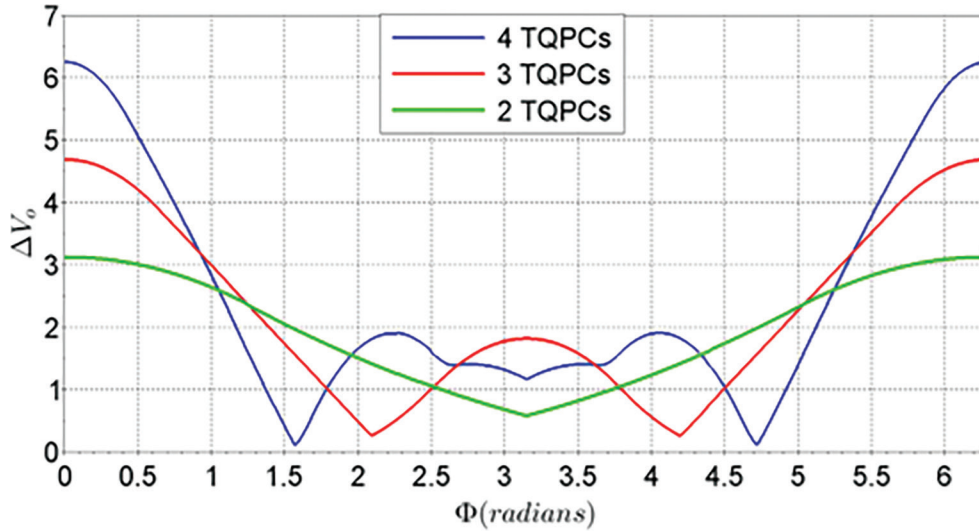


Fig. 4. Variation of ΔV_o as a function of Φ for phase-staggered operation of two, three, and four TQPCs in series. TQPCs, two-quadrant power converters.

Number of TQPCs in series	Phase shift with respect to TQPC ₁			
	TQPC ₂	TQPC ₃	TQPC ₄	TQPC _n
2	π	-	-	-
3	$2\pi/3$	$4\pi/3$	-	-
4	$\pi/2$	π	$3\pi/2$	-
n	$2\pi/n$	$4\pi/n$	$6\pi/n$	$2(n-1)\pi/n$

TQPCs, two-quadrant power converters.

Table 2. Value of optimum value of phase shift (Φ_{opt}) that results in minimum ΔV_o in phase-staggered series-connected TQPCs.

that the frequency of $\tilde{v}_o(t)$ is n times that of $\tilde{v}_i(t)$. Phase staggering, thus, in general results in reducing the filtering requirements and therefore the values of the filter components, which in turn, would improve the overall dynamic performance.

Next, for operation at $\Phi = \Phi_{opt}$, the variation of ΔV_o with D is calculated for two, three, and four phase-staggered series-connected TQPCs and is shown in Figure 5. It can be observed from Figure 5 that ΔV_o is maximum at certain duty cycles ($D_{\Delta V_{omax}}$) and minimum at certain duty cycles ($D_{\Delta V_{omin}}$). These results, along with generalisation to phase-staggered series-connected n TQPCs operating in the 1st and 2nd quadrants, are summarised in Tables 3 and 4, respectively.

4. Series-Connected Phase-Staggered TQPCs: Non-Ideal Case

Practically, it is difficult to maintain each TQPC identical in all respects as envisaged in the ideal case. There will be filter component tolerances, unequal input DC voltage of TQPCs, unequal duty cycles, and unequal on-state voltage drops in semiconductor devices. These non-ideal conditions cause deviation, as compared to the ideal-case calculations performed in the previous section, in ΔV_i and in turn, ΔV_o . It is indispensable for the designer to quantify these deviations in ΔV_o to incorporate such non-ideal conditions, so that the overall ripple of the power converter in the series-connected TQPCs remains within specified limits. The effects of these non-ideal conditions are calculated for the case of two series-connected TQPCs operating at $\Phi = \Phi_{opt}$, first individually and then in the cumulative manner.

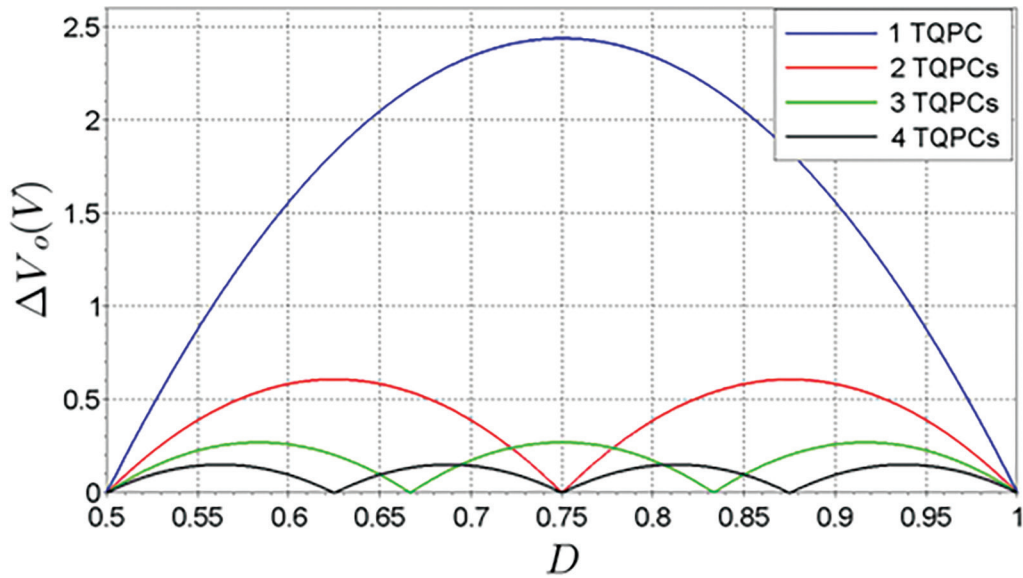


Fig. 5. Variation of ΔV_o as a function of D with $\Phi = \Phi_{opt}$ in two, three, and four phase-staggered series-connected TQPCs. TQPCs, two-quadrant power converters.

No. of TQPCs in series	$D_{\Delta V_{omin}}$	$D_{\Delta V_{omax}}$
	1st Quadrant	
2	0.5, 0.75, 1	0.625, 0.875
3	0.5, 0.67, 0.83, 1	0.585, 0.75, 0.915
4	0.5, 0.625, 0.75, 0.875, 1	0.5625, 0.6875, 0.8125, 0.9375
n	$0.5, 0.5\left(1 + \frac{1}{n}\right), 0.5\left(1 + \frac{2}{n}\right), \dots, 0.5\left(1 + \frac{i}{n}\right), \dots, 0.5\left(1 + \frac{n-1}{n}\right), 1$	$0.5\left(1 + \frac{1}{2n}\right), 0.5\left(1 + \frac{3}{2n}\right), \dots, 0.5\left(1 + \frac{2i-1}{n}\right), \dots, 0.5\left(1 + \frac{2n-1}{2n}\right)$

TQPCs, two-quadrant power converters.

Table 3. Values of $D_{\Delta V_{omin}}$ and $D_{\Delta V_{omax}}$ in 1st quadrant phase-staggered series-connected TQPCs.

No of TQPCs in series	$D_{\Delta V_{omin}}$	$D_{\Delta V_{omax}}$
	2nd Quadrant	
2	0, 0.25, 0.5	0.125, 0.375
3	0, 0.17, 0.33, 0.5	0.085, 0.25, 0.415
4	0, 0.125, 0.25, 0.375, 0.5	0.0625, 0.1875, 0.3125, 0.4375
n	$0, 0.5\left(\frac{1}{n}\right), 0.5\left(\frac{2}{n}\right), \dots, 0.5\left(\frac{i}{n}\right), \dots, 0.5\left(\frac{n-1}{n}\right), 0.5$	$0.5\left(\frac{1}{2n}\right), 0.5\left(\frac{3}{2n}\right), \dots, 0.5\left(\frac{2i-1}{2n}\right), \dots, 0.5\left(\frac{2n-1}{2n}\right)$

TQPCs, two-quadrant power converters.

Table 4. Values of $D_{\Delta V_{omin}}$ and $D_{\Delta V_{omax}}$ in 2nd quadrant phase-staggered series-connected TQPCs.

4.1. Effect of filter component tolerances

The filter components (inductor and capacitors) of the series-connected TQPCs could be different either due to manufacturing tolerances or due to unequal variation in their values with time or with operating conditions. For the case of two series-connected TQPCs, an analysis for the effect of $L_1 \neq L_2$, $C_1 \neq C_2$ is performed assuming components' values as per following cases and with rest of the parameters as per Table 1.

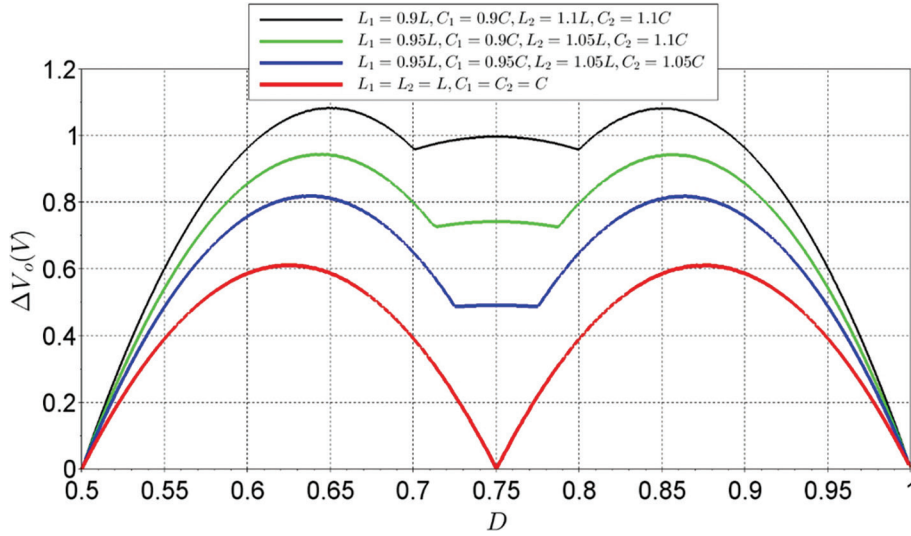


Fig. 6. Variation of ΔV_o as a function of D for two series-connected TQPCs with tolerances in filter inductor and capacitor values. TQPCs, two-quadrant power converters.

- Case 1: Inductor and capacitor of TQPC₁ are assumed to be having -10% tolerance. Inductor and capacitor of TQPC₂ are assumed to be having $+10\%$ tolerance. This is the worst case when $\pm 10\%$ tolerances are considered. ($L_1 = 0.9 \times 80 \mu\text{H}$, $C_1 = 0.9 \times 20 \mu\text{F}$; $L_2 = 1.1 \times 80 \mu\text{H}$, $C_2 = 1.1 \times 20 \mu\text{F}$)
- Case 2: Inductor and capacitor of TQPC₁ are assumed to be having -5% and -10% tolerance, respectively. Inductor and capacitor of TQPC₂ are assumed to be having $+5\%$ and $+10\%$ tolerance, respectively. This is the worst case when $\pm 5\%$ and $\pm 10\%$ tolerances are considered in inductor and capacitor, respectively. ($L_1 = 0.95 \times 80 \mu\text{H}$, $C_1 = 0.9 \times 20 \mu\text{F}$; $L_2 = 1.05 \times 80 \mu\text{H}$, $C_2 = 1.1 \times 20 \mu\text{F}$)
- Case 3: Inductor and capacitor of TQPC₁ are assumed to be having -5% tolerance. Inductor and capacitor of TQPC₂ are assumed to be having $+5\%$ tolerance. This is the worst case when $\pm 5\%$ tolerances are considered. ($L_1 = 0.95 \times 80 \mu\text{H}$, $C_1 = 1.05 \times 20 \mu\text{F}$; $L_2 = 0.95 \times 80 \mu\text{H}$, $C_2 = 1.05 \times 20 \mu\text{F}$).

In each case, the waveform of $\tilde{v}_1(t)$ is obtained using Eq. (3) with TQPC₁ filter component values. The waveform of $\tilde{v}_2(t)$ is also obtained using Eq. (3) with TQPC₂ filter component values and shifting it in the time domain by an amount that results in $\Phi = \pi$. Then, $\tilde{v}_o(t)$ is obtained from the addition of $\tilde{v}_1(t)$ and $\tilde{v}_2(t)$. ΔV_o is obtained from the difference of maxima and minima of $\tilde{v}_o(t)$. The plots of variation of ΔV_o as a function of D for Cases 1, 2, and 3, as well as for the ideal case, are shown in Figure 6. The plot for the ideal case is also shown for reference. It can be observed that the deviation in ΔV_o from the ideal case is directly proportional to the deviation of the L and C values from the ideal case.

4.2. Effect of unequal input DC voltages

In practice, the input DC voltages of series-connected TQPCs may not be equal. For the case of two series-connected TQPCs, analysis for the effect of $V_{\text{DC1}} \neq V_{\text{DC2}}$ is performed with input DC voltage values as per following cases and other parameters as per Table 1.

- Case 1: Input DC voltage of TQPC₁ is assumed to be 10% higher than the nominal value of V_{DC} (given in Table 1) and that of TQPC₂ is assumed to be 10% lower than the nominal value of V_{DC} .
- Case 2: Input DC voltage of TQPC₁ is assumed to be 5% higher than the nominal value of V_{DC} (given in Table 1) and that of TQPC₂ is assumed to be 5% lower than the nominal value of V_{DC} .

In each case, the waveform of $\tilde{v}_1(t)$ is obtained using Eq. (3) with the input DC voltage of V_{DC1} . Further, the waveform of $\tilde{v}_2(t)$ is also obtained from Eq. (3) with the input DC voltage of V_{DC2} and shifting it in the time domain by an amount that results in $\Phi = \pi$. As before, $\tilde{v}_o(t)$ is obtained from the addition of $\tilde{v}_1(t)$ and $\tilde{v}_2(t)$ and ΔV_o is obtained from the difference of maxima and minima of $\tilde{v}_o(t)$. The plots of variation of ΔV_o as a function of D for Cases 1 and 2,

as well as for the ideal case, are shown in Figure 7. It can be observed that ΔV_o is strongly dependent on the amount of variation in the input DC voltages.

4.3. Effect of unequal duty cycle

Although the series-connected TQPCs are assumed to operate with common duty-cycle control, the duty cycle of the control pulses seen by the semiconductor switches in different TQPCs could be different. This difference may be attributed to the variations in the individual pulse generation circuits due to component tolerances, unequal propagation delay times, rise/fall times of the driver cards, etc. The measured performance of driver cards (Kamaria, 2011) suggests that a typical variation of approximately 400 ns in the on-time of the switches can be expected. In concomitance with a 10 kHz switching frequency, this results in the expected variation of duty cycle being obtained at the order of 0.004. The waveform of $\tilde{v}_1(t)$ is obtained using Eq. (3) with TQPC₁ duty cycle ($D_1 = D - 0.004$). Further, the waveform of $\tilde{v}_2(t)$ is obtained using Eq. (3) with TQPC₂ duty cycle $D_2 = D$ and by shifting it in the time domain by an amount that results in $\Phi = \pi$. Then $\tilde{v}_o(t)$ is obtained from the addition of $\tilde{v}_1(t)$ and $\tilde{v}_2(t)$. ΔV_o is obtained from the difference of maxima and minima of $\tilde{v}_o(t)$. ΔV_o is plotted as a function of D and compared with the ideal case $D_1 = D_2 = D$, as shown in Figure 8.

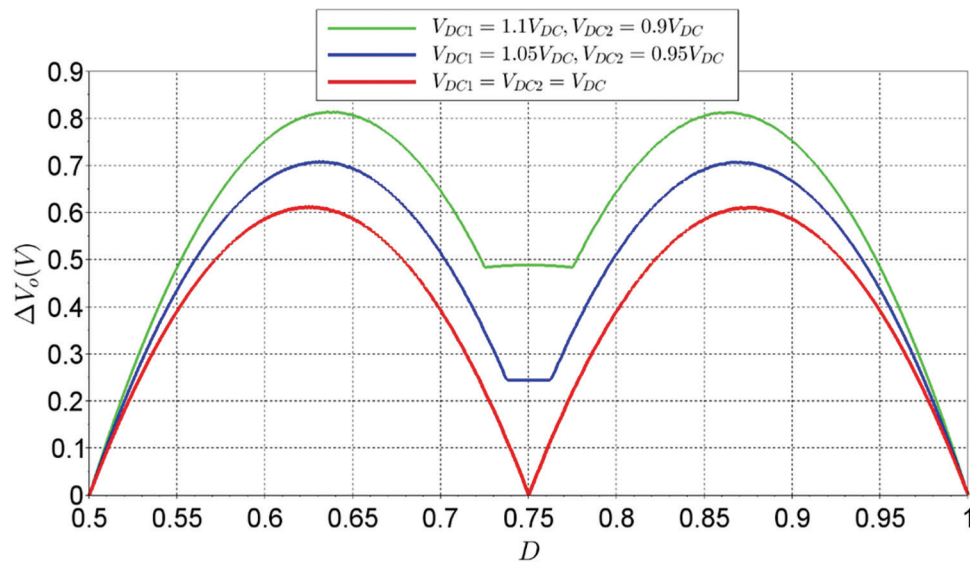


Fig. 7. Variation of ΔV_o as a function of D for two series-connected TQPCs characterised by unequal input DC voltages. TQPCs, two-quadrant power converters.

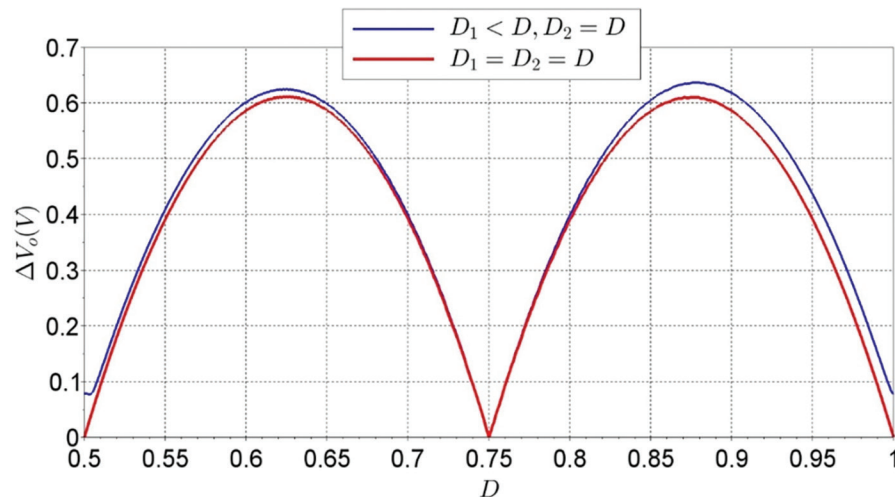


Fig. 8. Variation of ΔV_o as a function of D for two series-connected TQPCs with unequal duty cycles. TQPCs, two-quadrant power converters.

4.4. Effect of unequal on-state voltage drops in IGBT and diode

On-state voltage drops in semiconductor devices are provided in datasheet as minimum, typical, and maximum values. Besides, these values vary strongly with the junction temperature. Therefore, the devices are expected to exhibit unequal voltage drops. Worst case variations in on-state voltage drops are considered from the datasheets (SPT IGBT Module datasheet, 2006) of diode and insulated-gate bipolar transistor (IGBT,) and the following cases are considered for analysis:

- Case 1: IGBT voltage drop $V_{s1} = 1.6V$ and diode voltage drop $V_{d1} = 1.7V$ for TQPC₁, and IGBT voltage drop $V_{s2} = 1.95V$ and diode voltage drop $V_{d2} = 2V$ for TQPC₂.
- Case 2: IGBT voltage drop and diode voltage drop $V_{s1} = V_{s2} = 1.6V$, $V_{d1} = V_{d2} = 1.7V$ are equal for both the TQPCs (ideal case).

The waveform of $\tilde{v}_1(t)$ is obtained using Eq. (3). In this specific case, IGBT and diode voltage drop of TQPC₁ are considered while computing ΔI_L , whose expression is given by:

$$\Delta I_L = \begin{cases} \frac{(V_{DC} - V_s + V_d)(1-D)(2D-1)}{L} & \text{1st quadrant operation} \\ \frac{(V_{DC} - V_s + V_d)D(1-2D)}{L} & \text{2nd quadrant operation} \end{cases} \quad (6)$$

where V_s and V_d represent IGBT and diode voltage drop, respectively.

Further, the waveform of $\tilde{v}_2(t)$ is obtained using Eq. (3) and by shifting it in the time domain by an amount that results in $\phi = \pi$. In this case, too, IGBT and diode voltage drop of TQPC₂ are considered while computing ΔI_L as given by Eq. (6). As before, $\tilde{v}_o(t)$ is obtained from the addition of $\tilde{v}_1(t)$ and $\tilde{v}_2(t)$, and ΔV_o is obtained from the difference of maxima and minima of $\tilde{v}_o(t)$. The plots of variation of ΔV_o as a function of D for Cases 1 and 2 are shown in Figure 9.

4.5. Cumulative effect

The cumulative effect of the above-mentioned non-ideal conditions is illustratively calculated, considering the following set of parameters:

- $V_{DC1} = 1.05 \times 50 \text{ V}$, $V_{DC2} = 0.95 \times 50 \text{ V}$
- $L_1 = 0.9 \times 80 \mu\text{H}$, $L_2 = 1.1 \times 80 \mu\text{H}$, $C_1 = 0.9 \times 20 \mu\text{F}$, $C_2 = 1.1 \times 20 \mu\text{F}$

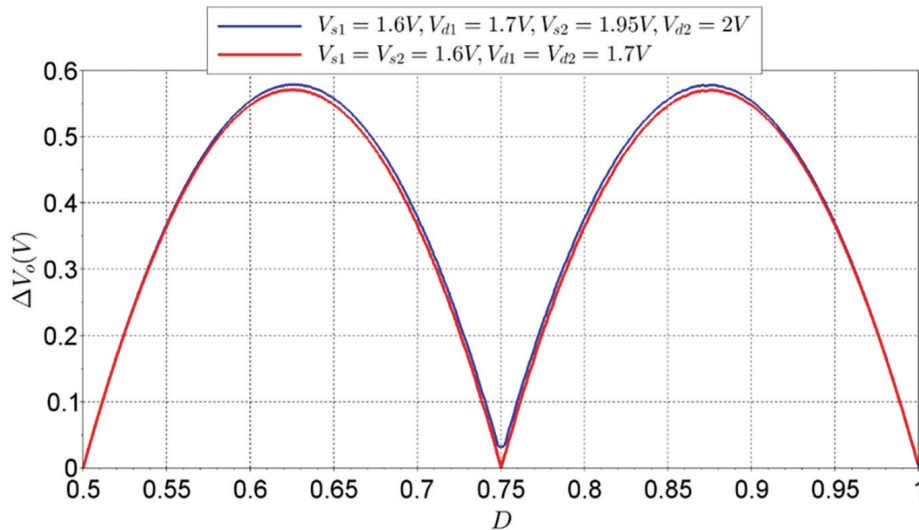


Fig. 9. Variation of ΔV_o as a function of D for two series-connected TQPCs with unequal on-state switch voltage drop. TQPCs, two-quadrant power converters.

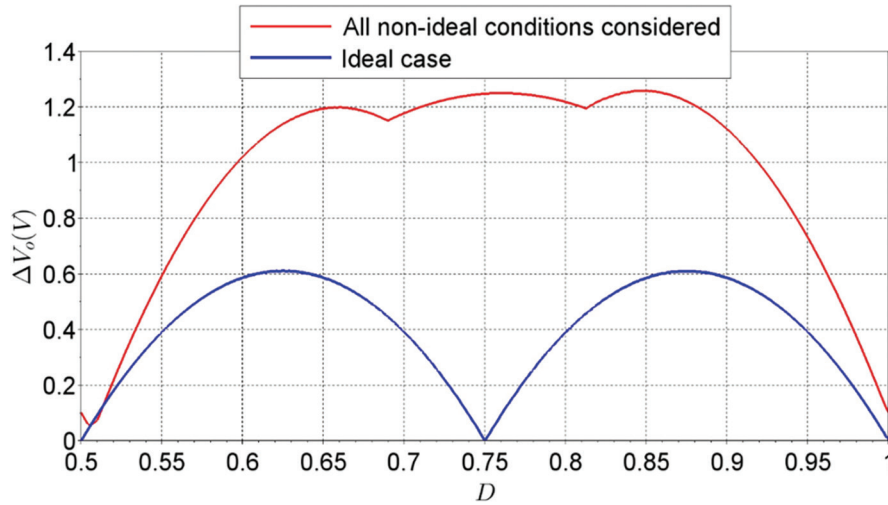


Fig. 10. Variation of ΔV_o as a function of D for two series-connected TQPCs considering the cumulative effect of various non-ideal conditions. TQPCs, two-quadrant power converters.

- IGBT voltage drop $V_{s1} = 1.6V$ and diode voltage drop $V_{d1} = 1.7V$ for TQPC₁, IGBT voltage drop $V_{s2} = 1.95V$ and diode voltage drop $V_{d2} = 2V$ for TQPC₂
- Inclusion of variation of D

The waveform of $\tilde{v}_1(t)$ is obtained using Eq. (3) considering parameters of TQPC₁ and duty cycle ($D_1 = D - 0.004$). Further, the waveform of $\tilde{v}_2(t)$ is obtained using Eq. (3) with TQPC₂ parameters and by shifting it in the time domain by an amount that results in $\Phi = \pi$. In this analysis, IGBT and diode voltage drop of TQPC are considered while computing ΔI_L as given by Eq. (6). Then, $\tilde{v}_o(t)$ is obtained from the addition of $\tilde{v}_1(t)$ and $\tilde{v}_2(t)$. ΔV_o is obtained from the difference of maxima and minima of $\tilde{v}_o(t)$. The plots of variation of ΔV_o as a function of D for the non-ideal and ideal cases are shown in Figure 10.

It can be observed from Figures 6 and 7 that the deviation of ΔV_o from the ideal case is directly proportional to the deviation of the L and C values and V_{DC} from the ideal case. This emphasises the importance of having little or very less deviation in L , C , and V_{DC} for each TQPC. Further, it can be observed from Figures 8 and 9 that the effect of unequal on-state voltage drops in IGBT and diode and $D_1 \neq D_2$ on ΔV_o is not significant. Thus, their effect on ΔV_o can be neglected as a part of valid approximation.

5. Simulation and Experimental Verification

Simulation and experimental demonstration are carried out in order to verify the analysis performed in earlier sections.

5.1. Simulation verification

Simulation is performed in Cadence Design Systems OrCAD PSpice Designer software 17.2 in order to validate the analytical framework developed in the preceding sections. The simulation circuit consists of TQPCs connected in series, as shown in Figure 1 ($n = 2$). Simulation verification is performed for the ideal case, and the parameters used for the corresponding purpose are those provided in Table 1. Waveforms of $\tilde{v}_1(t)$, $\tilde{v}_2(t)$, and $\tilde{v}_o(t)$ for various duty cycles ($D = 0.525, 0.55, \dots, 0.975$) obtained from simulation are shown in Figure 11.

ΔV_o is acquired from the peak-peak ripple voltage of $\tilde{v}_o(t)$ from the waveforms of $\tilde{v}_o(t)$ for $D = 0.525, 0.55, \dots, 0.975$. The plot of variation of ΔV_o as a function of D for two series-connected TQPCs in phase-staggering mode obtained from Eq. (3) and PSpice simulation is as shown in Figure 12.

Verification of the effect of tolerance in filter component values is carried out assuming inductor and capacitor values as $L_1 \neq L_2$, $C_1 \neq C_2$ and having tolerance in the range (± 10). As the worst case combination, the filter components (inductor and capacitors) considered for simulation are $L_1 = 72 \mu H$, $C_1 = 18 \mu F$, $L_2 = 88 \mu H$, and $C_2 = 22 \mu F$.

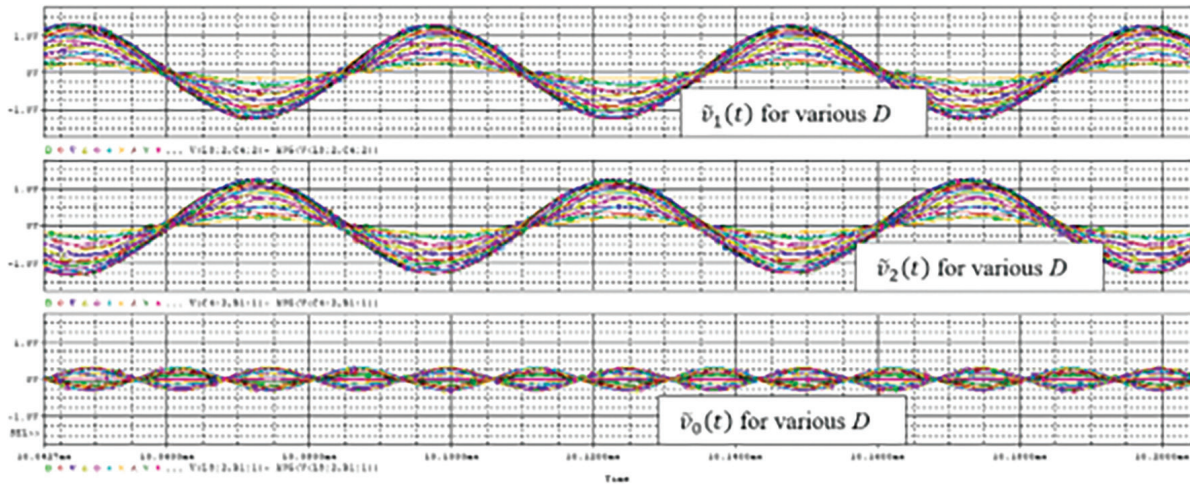


Fig. 11. Waveforms of $\tilde{v}_1(t)$, $\tilde{v}_2(t)$, and $\tilde{v}_o(t)$ for two series-connected TQPCs at various D varying from 0.525 to 0.975 with phase-staggered operation under ideal conditions. TQPCs, two-quadrant power converters.

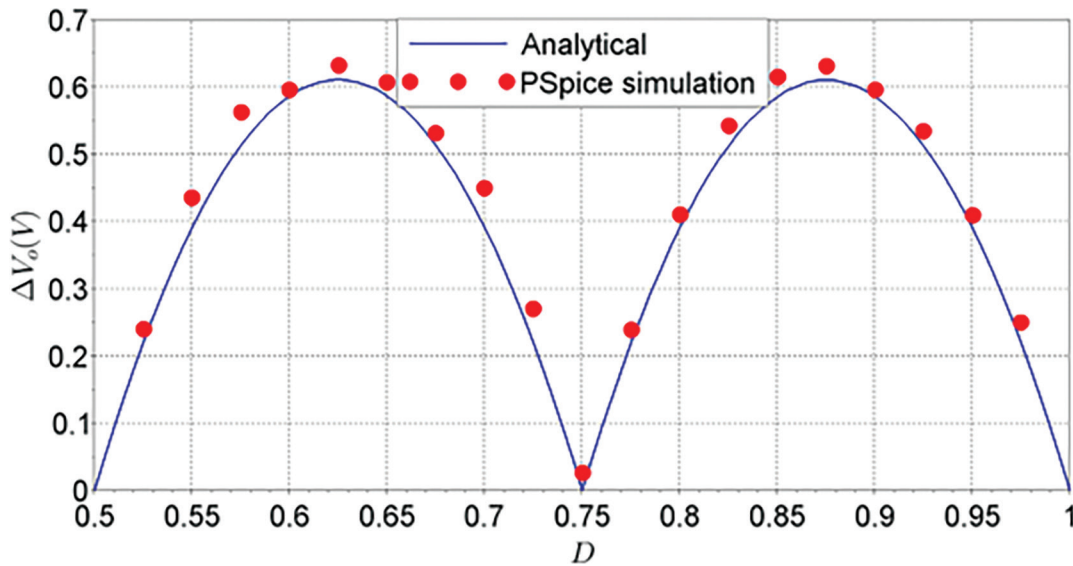


Fig. 12. Variation of ΔV_o as a function of D for two series-connected TQPCs for the ideal case obtained from analysis and PSpice simulation. TQPCs, two-quadrant power converters.

Other parameters remain the same as per Table 1. Waveforms of $\tilde{v}_1(t)$, $\tilde{v}_2(t)$, and $\tilde{v}_o(t)$ for various duty cycles ($D = 0.525, 0.55, \dots, 0.975$) obtained from simulation are shown in Figure 13. It can be observed that ΔV_o has increased as compared to the ideal case. As before, ΔV_o is acquired from the peak–peak ripple voltage of $\tilde{v}_o(t)$ waveforms. Variation of ΔV_o as a function of D for two series-connected TQPCs in phase-staggering mode and with unequal filter components obtained from Eq. (3) and PSpice simulation is shown in Figure 14.

Next, the verification of the effect of unequal input DC voltages is performed assuming input DC voltages as $V_{DC1} \neq V_{DC2}$ with the tolerance of ($\pm 5\%$). Input DC voltages of the two TQPCs considered for simulation are $V_{DC1} = 52.5\text{ V}$ and $V_{DC2} = 47.5\text{ V}$. Other parameters remain the same as per Table 1. Waveforms of $\tilde{v}_1(t)$, $\tilde{v}_2(t)$, and $\tilde{v}_o(t)$ for various duty cycles ($D = 0.525, 0.55, \dots, 0.975$) obtained from simulation are shown in Figure 15. It can be observed that ΔV_o has increased as compared to the ideal case. As before, ΔV_o is acquired from the peak–peak ripple voltage of $\tilde{v}_o(t)$ waveforms. Variation of ΔV_o as a function of D for two series-connected TQPCs in phase-staggering mode with unequal DC voltages obtained from Eq. (3) and PSpice simulation is shown in Figure 16.

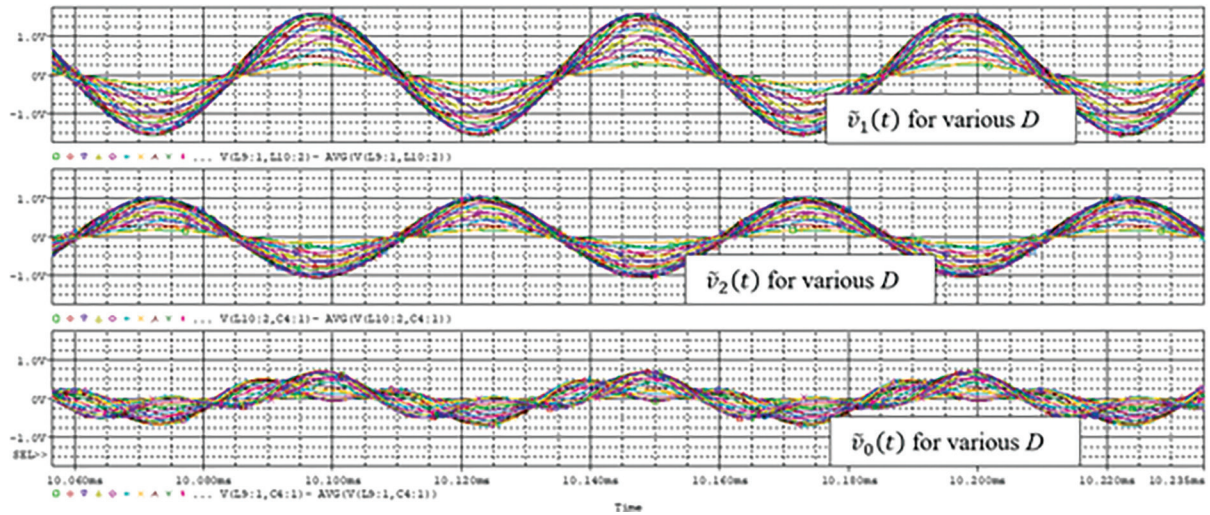


Fig. 13. Waveforms of $\tilde{v}_1(t)$, $\tilde{v}_2(t)$, and $\tilde{v}_o(t)$ for two series-connected TQPCs at various D varying from 0.525 to 0.975 with phase-staggered operation under filter component tolerances. TQPCs, two-quadrant power converters.

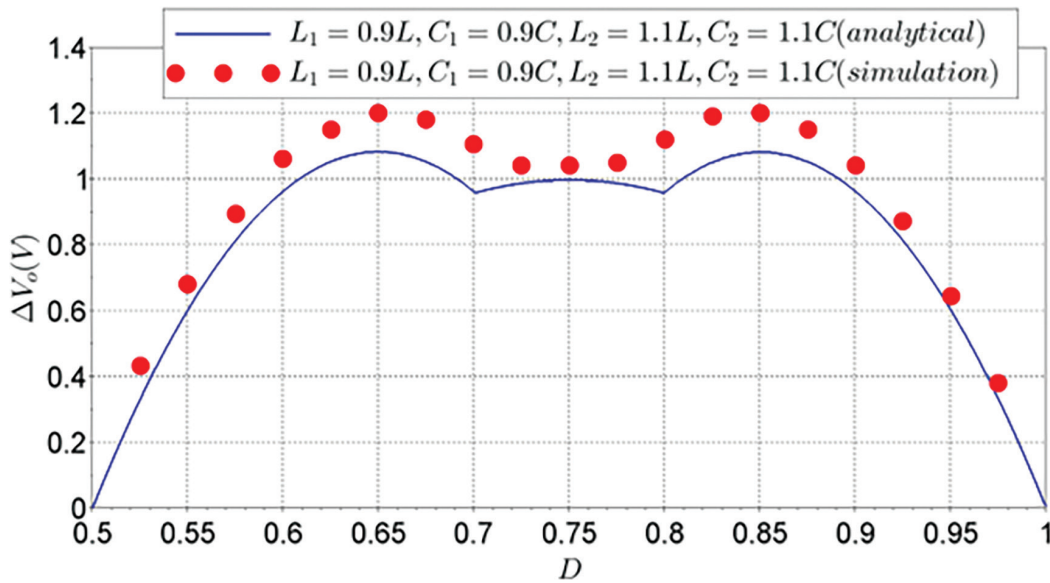


Fig. 14. Variation of ΔV_o as a function of D for two series-connected TQPCs for $L_1 \neq L_2$, $C_1 \neq C_2$ ($\pm 10\%$) obtained from analysis and PSpice simulation. TQPCs, two-quadrant power converters.

To visualise the integrated effect, simulations are carried out to incorporate the effects of both filter component tolerances ($\pm 10\%$) and unequal input DC voltages ($\pm 5\%$). $L_1 = 72 \mu H$, $C_1 = 18 \mu F$, $L_2 = 88 \mu H$, $C_2 = 22 \mu F$, $V_{DC1} = 52.5V$, and $V_{DC2} = 47.5V$ are the values considered for the simulation. Waveforms of $\tilde{v}_1(t)$, $\tilde{v}_2(t)$, and $\tilde{v}_o(t)$ for various duty cycles ($D = 0.525$ to 0.975) obtained from simulation are shown in Figure 17. As before, ΔV_o is acquired from the peak–peak ripple voltage of $\tilde{v}_o(t)$ waveforms. Variation of ΔV_o as a function of D for two series-connected TQPCs in phase-staggering mode with $L_1 \neq L_2$, $C_1 \neq C_2$ ($\pm 10\%$), and $V_{DC1} \neq V_{DC2}$ ($\pm 5\%$), as obtained from analysis and PSpice simulation, is shown in Figure 18. It can be observed that the simulation and analytical results are closely matching.

In Figures 12, 14, 16, and 18, the blue line represents analytical results that are obtained with certain simplified assumptions. In these results, on-state voltage drops of IGBT and diode are not considered. On the other hand, the device models used/available in PSpice simulation have non-zero voltage drops. These drops become significant, particularly in low output voltage design. The slightly higher value of voltage ripple observed in simulation can be

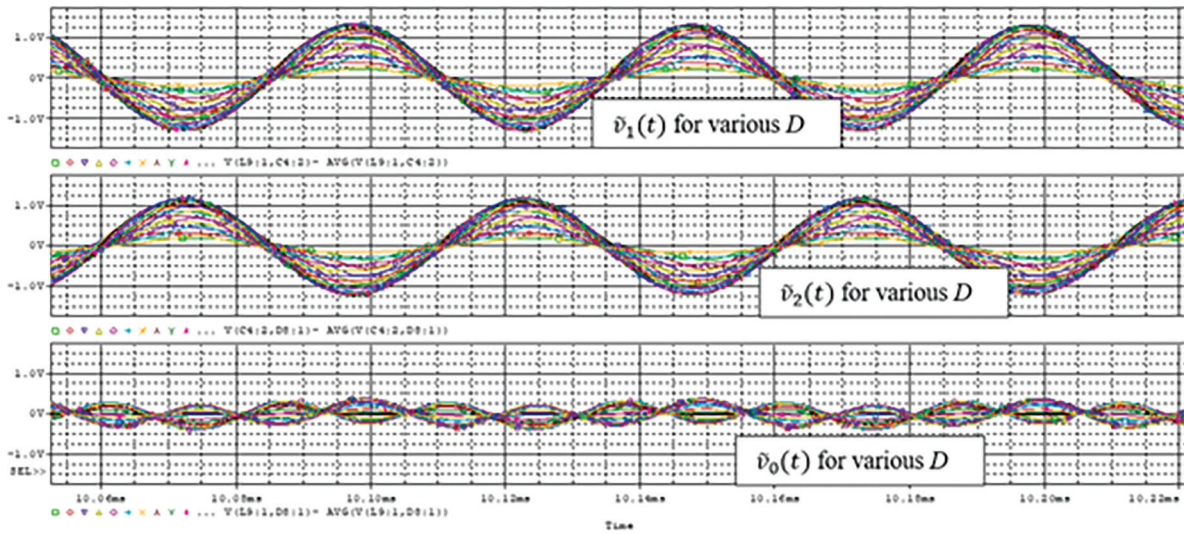


Fig. 15. Waveforms of $\bar{v}_1(t)$, $\bar{v}_2(t)$, and $\bar{v}_0(t)$ for two series-connected TQPCs at various D varying from 0.525 to 0.975 with phase-staggered operation under unequal input DC voltages. TQPCs, two-quadrant power converters.

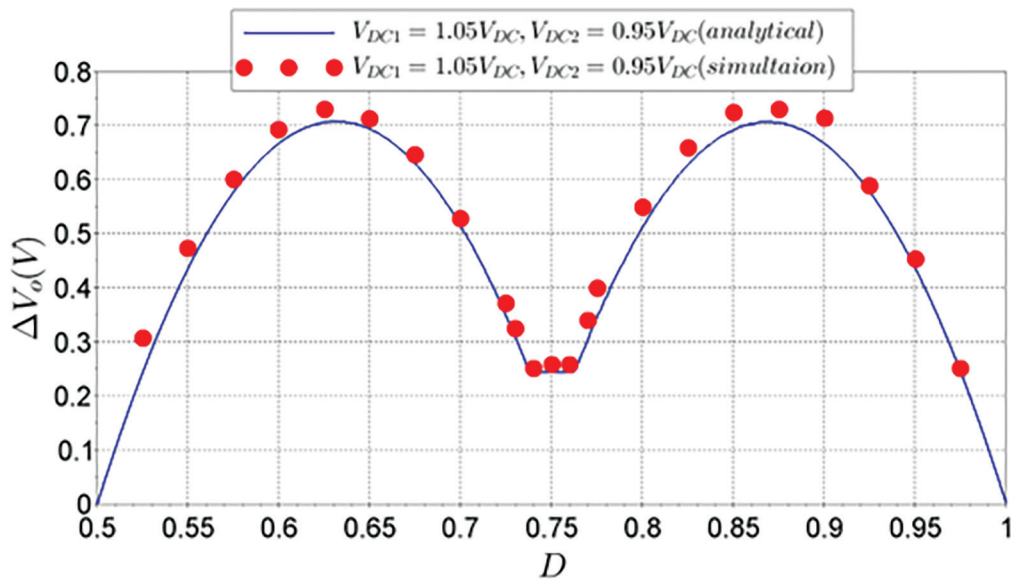


Fig. 16. Variation of ΔV_0 as a function of D for two series-connected TQPCs for $V_{DC1} \neq V_{DC2} (\pm 5\%)$ obtained from analysis and PSpice simulation. TQPCs, two-quadrant power converters.

attributed to this reason. However, the maximum error between analytical and simulation results lies between 5% and 15%.

5.2. Experimental verification

An experimental setup, having two stages of TQPCs (operating from 50 V DC input and rated to deliver 100 A, 35 V maximum output) connected in series, was developed to verify the analysis presented in the previous sections. A block diagram of experimental setup is depicted in Figure 19. TQPC is used to provide output current to magnet load. Each stage of TQPC is preceded by two-switch forward converters (TSFC). The TSFC at the front end of TQPC is used for varying the voltage (up to a maximum value of 70 V) across the intermediate DC-link storage capacitor. A three-phase AC–DC converter (diode rectifier and filter) provides input DC to the TSFC. An intermediate DC-link capacitor is used for energy-storage purpose. Reference voltage V_{ref} for both TSFCs can be varied during the experiment to vary the output voltage of two TSFCs. Duty cycle of TQPCs and phase-shift in TQPC₂ for

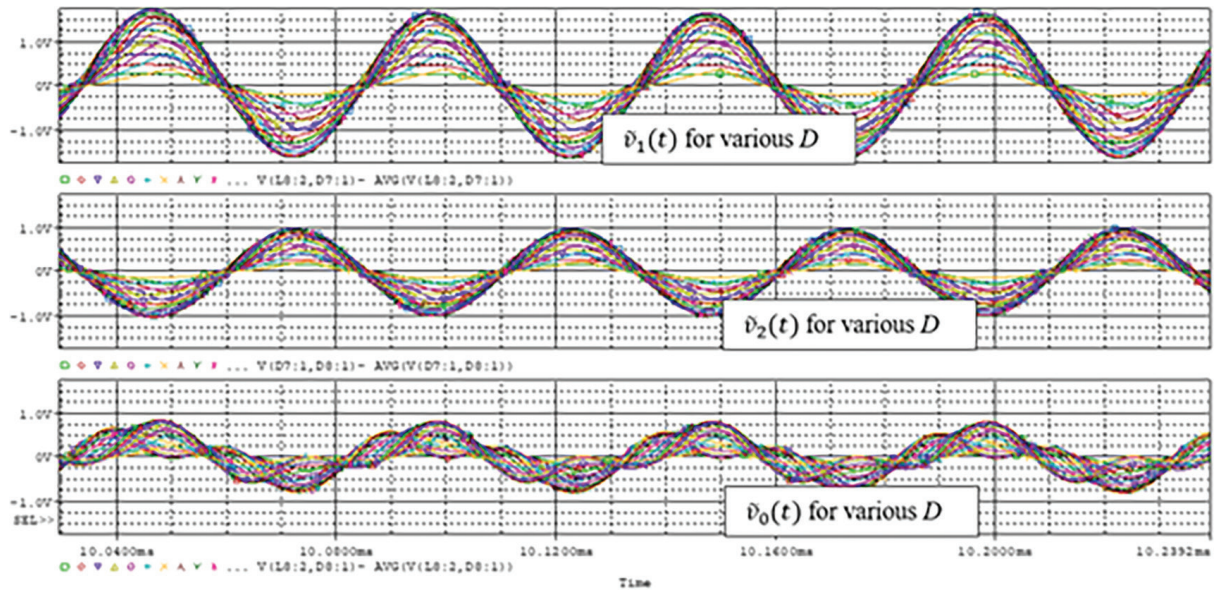


Fig. 17. Waveforms of $\tilde{v}_1(t)$, $\tilde{v}_2(t)$, and $\tilde{v}_0(t)$ for two series-connected TQPCs at various D varying from 0.525 to 0.975 with phase-staggered operation under filter component tolerances and unequal input DC voltages. TQPCs, two-quadrant power converters.

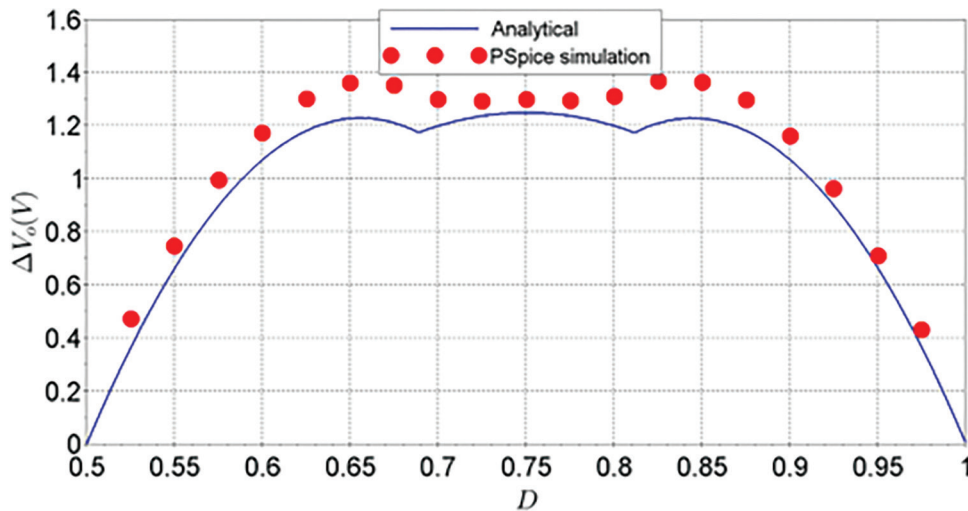


Fig. 18. Variation of ΔV_0 as a function of D for two series-connected TQPCs for $L_1 \neq L_2$, $C_1 \neq C_2$ ($\pm 10\%$), and $V_{DC1} \neq V_{DC2}$ ($\pm 5\%$) obtained from analysis and PSpice simulation. TQPCs, two-quadrant power converters.

phase-staggering mode are varied using a common TQPC control card. The circuit diagram of an individual TQPC can be seen in Figure 1. In TQPC, the switches carry the full load current (100 A maximum). Thus, IGBT is chosen as a semiconductor switch in TQPC. The circuit diagram of TSFC is shown in Figure 20, wherein V_{in} is the input voltage to TSFC taken from the AC–DC power supply. Since the transformer T_{x2} is a step down transformer, the switches M_1 , M_2 in TSFC carry comparatively less current but need to block the high DC-link voltage. Therefore, MOSFETs are used as switches M_1 , M_2 . The filter inductor L and the energy-storage capacitors $C_{DC1/DC2}$ constitute the low-pass filter in TSFC. Independent control cards are used for controlling the output voltage of TSFCs. The block diagram of a TSFC control card is shown in Figure 21. In the TSFC control card, proportional controller and pulse width modulation scheme are used. $G_{c1}(s)$ is a compensator transfer function, $G_{PWM}(s)$ is the transfer function of the pulse width modulator, $G_{of}(s)$ is the control to output voltage transfer function of the TSFC, and $H_1(s)$ is the sensor gain of feedback. The TQPC control card is used to control the output current of series-connected TQPCs. A common TQPC control card is used for both the TQPCs. The block diagram of a TQPC control card is shown in Figure 22. In

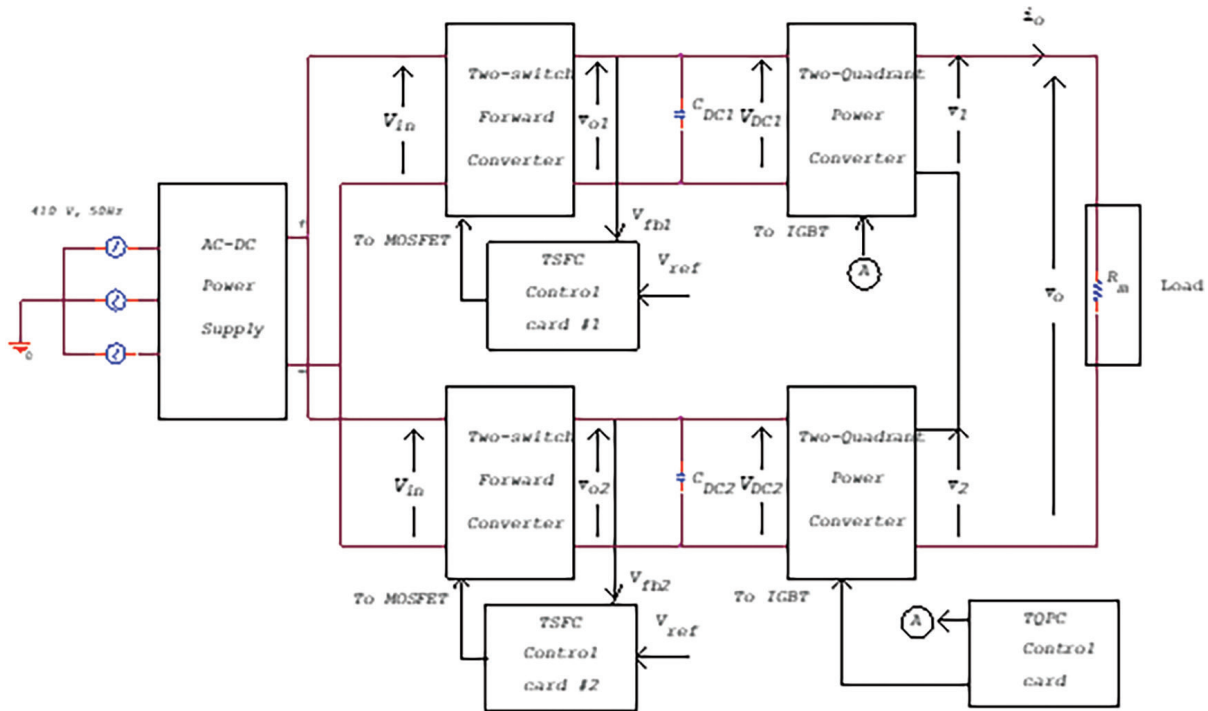


Fig. 19. Block diagram of experimental setup. TSFC, two-switch forward converters.

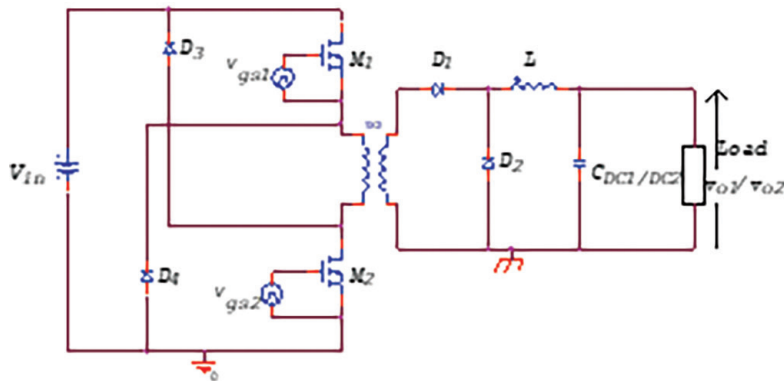


Fig. 20. Circuit diagram of TSFC. TSFC, two-switch forward converters.

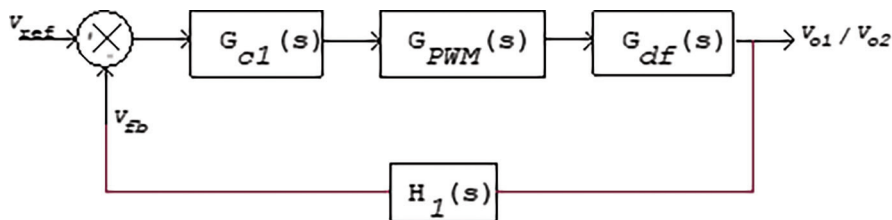


Fig. 21. Block diagram of TSFC control card. TSFC, two-switch forward converters.

the TQPC control card, a pole-zero compensation method is used to design the compensator, and a unipolar pulse width modulation scheme is used. $G_{c2}(s)$ is the compensator transfer function, $G_{UPWM}(s)$ is the transfer function of the unipolar pulse width modulator, $G_{di}(s)$ is the control to output current transfer function of the TQPC, and $H_2(s)$ is the sensor gain of feedback. A detailed description of the small-signal transfer function and the controller design following

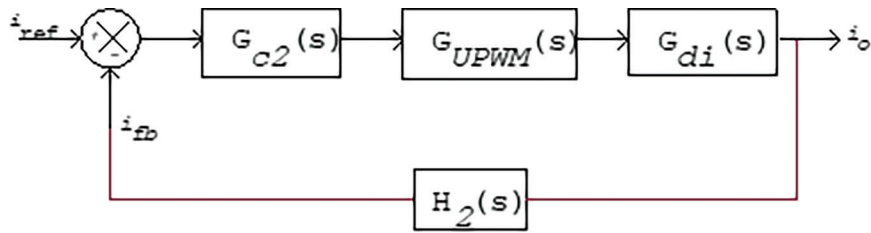


Fig. 22. Block diagram of TQPC control card. TQPC, two-quadrant power converter.

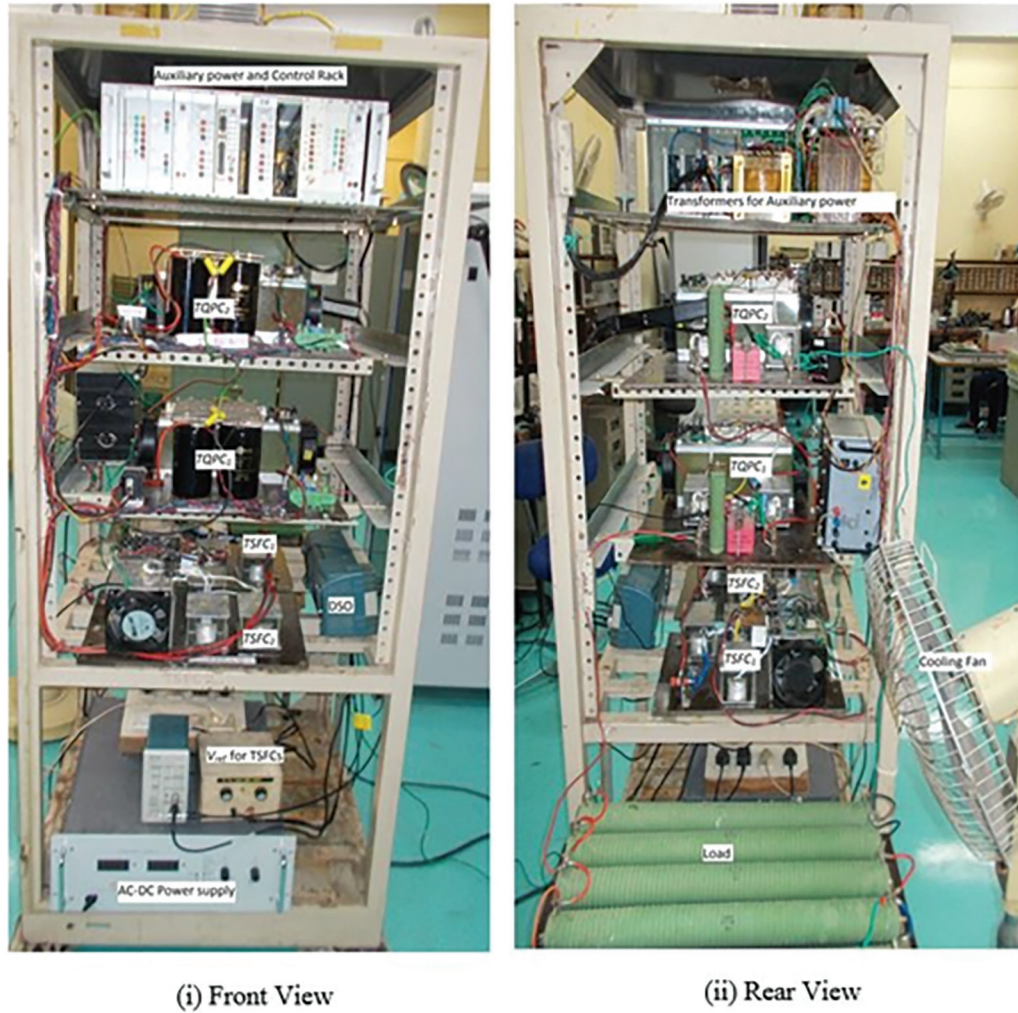


Fig. 23. Photograph of experimental setup.

the conventional techniques is provided in the study of Srivastava (2022). A photograph of the experimental setup is shown in Figure 23. An experimental verification of filter component tolerances would have required additional inductors and capacitors with certain specified values ($L_1 = 72 \mu\text{H}$, $C_1 = 18 \mu\text{F}$, $L_2 = 88 \mu\text{H}$, $C_2 = 22 \mu\text{F}$), which were difficult to source. Thus, experimental verification is carried out for unequal V_{DC} condition, which is felt adequate in relation to validation of the methodology.

At the outset, experimental verification of the ideal case is performed. For this, $V_{\text{DC1}} = V_{\text{DC2}} = 50\text{V}$ and $D = 0.6$ were the values used. The inductor and capacitor values were as per Table 1. Experimental waveforms \tilde{v}_1 , \tilde{v}_2 , and \tilde{v}_0 of two TQPCs in series in phase-staggering mode operating at $\Phi = \Phi_{\text{opt}}$ are shown in Figure 24. It may be noted that the waveforms are quite similar to the analytical prediction depicted in Figure 3a.

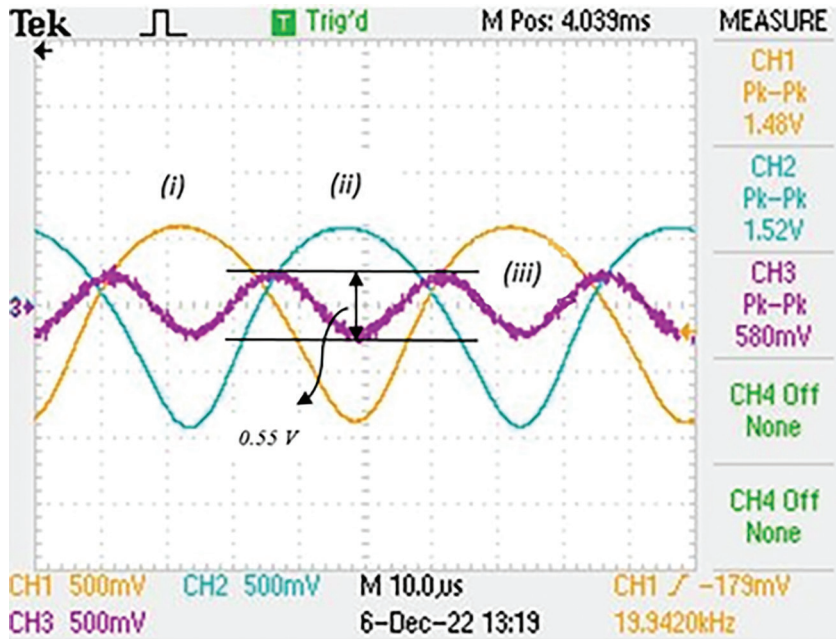


Fig. 24. Experimental waveforms of \tilde{v}_1 , \tilde{v}_2 , and \tilde{v}_0 for TQPCs in series in phase-staggering mode operating at $\Phi = \Phi_{opt}$; $D = 0.6$, $V_{DC1} = V_{DC2} = 50V$; (i) \tilde{v}_1 , 0.5 V/div, (ii) \tilde{v}_2 , 0.5 V/div, (iii) \tilde{v}_0 , 0.5 V/div; x axis, 10 μs /div. TQPCs, two-quadrant power converters.

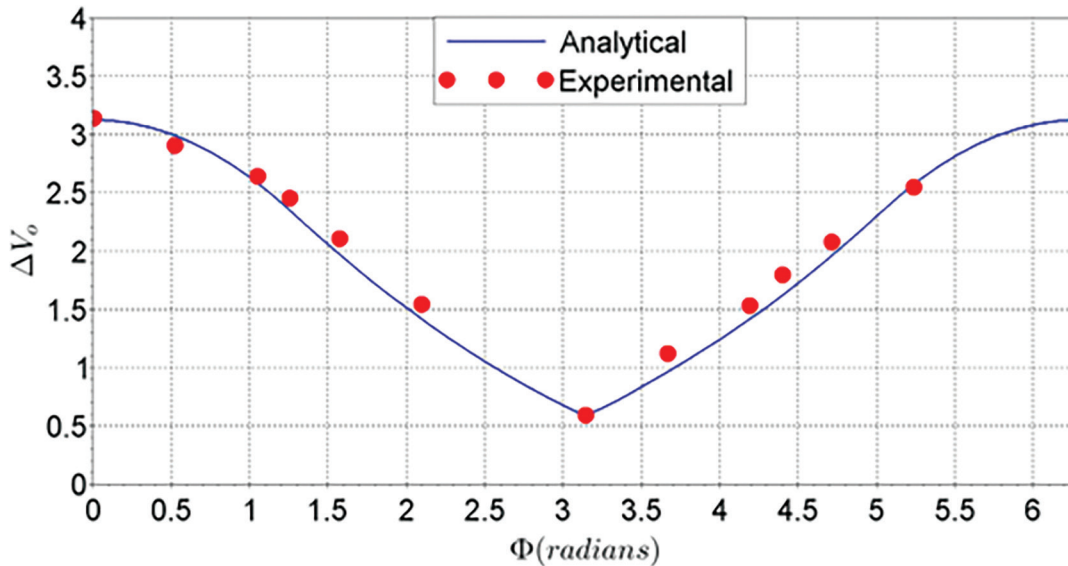


Fig. 25. Variation of ΔV_o as a function of Φ obtained from analysis and experimental results.

Phase-shifts of control gate pulses associated with TQPC₂ are varied in order to verify the variation of ΔV_o as a function of Φ . Waveforms of \tilde{v}_1 , \tilde{v}_2 , and \tilde{v}_0 are obtained for each phase-shift. ΔV_o is obtained from the difference between maxima and minima of \tilde{v}_0 . The plot of variation of ΔV_o as a function of Φ is shown in Figure 25, as obtained from analysis and experimental results. It can be seen that ΔV_o is minimum for $\Phi = \pi$.

The effect of duty cycle on ΔV_o is experimentally verified with phase-shift $\Phi = \Phi_{opt}$. Waveforms of \tilde{v}_1 , \tilde{v}_2 , and \tilde{v}_0 are obtained for each D . As before, ΔV_o is obtained from the difference between maxima and minima of \tilde{v}_0 . The plot of variation of ΔV_o as a function of D is shown in Figure 26, as obtained from analysis, experimental results and PSpice simulation.

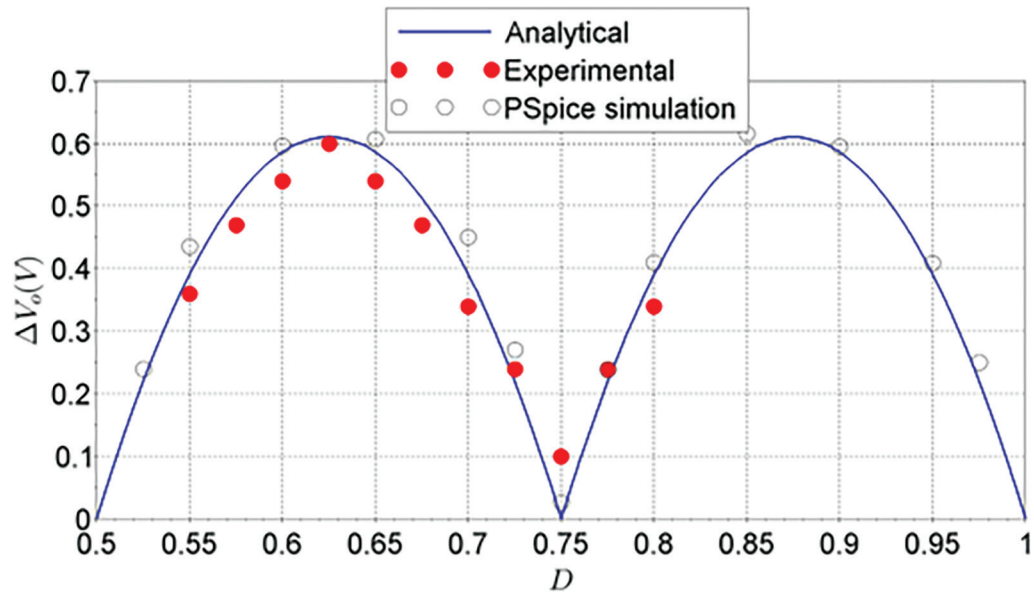


Fig. 26. Variation of ΔV_o as a function of D for TQPCs in series in phase-staggering mode operating at $\Phi = \Phi_{opt}$ obtained from analysis, experimental results and PSpice simulation. TQPCs, two-quadrant power converters.

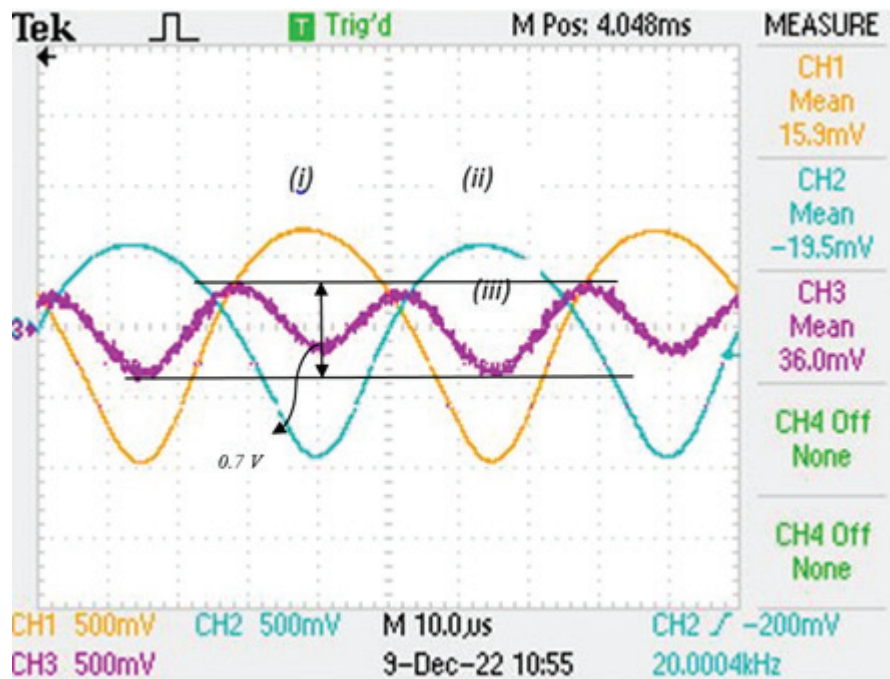


Fig. 27. Experimental waveforms of \tilde{v}_1 , \tilde{v}_2 , and \tilde{v}_0 for TQPCs in series in phase-staggering mode operating at $\Phi = \Phi_{opt}$ with $V_{DC1} \neq V_{DC2}$; $D = 0.6$, $V_{DC1} = 52.5V$, $V_{DC2} = 47.5V$; (i) \tilde{v}_1 , $0.5 V/div$, (ii) \tilde{v}_2 , $0.5 V/div$, (iii) \tilde{v}_0 , $0.5 V/div$; x axis, $10 \mu s/div$. TQPCs, two-quadrant power converters.

Experimental validation of the effect of non-ideality $V_{DC1} \neq V_{DC2}$ is performed. V_{DC1} and V_{DC2} are set to 52.5 V and 47.5 V, respectively. Experimental waveforms \tilde{v}_1 , \tilde{v}_2 , and \tilde{v}_0 of two TQPCs in series in phase-staggering mode operating at $\Phi = \Phi_{opt}$ with $D = 0.6$ are as shown in Figure 27. It can be observed from the figure that $\Delta V_1 > \Delta V_2$. Variation of ΔV_o as a function of D was obtained experimentally, and plot is shown in Figure 28. This figure shows the variation obtained from analysis, experimental results and PSpice simulation.

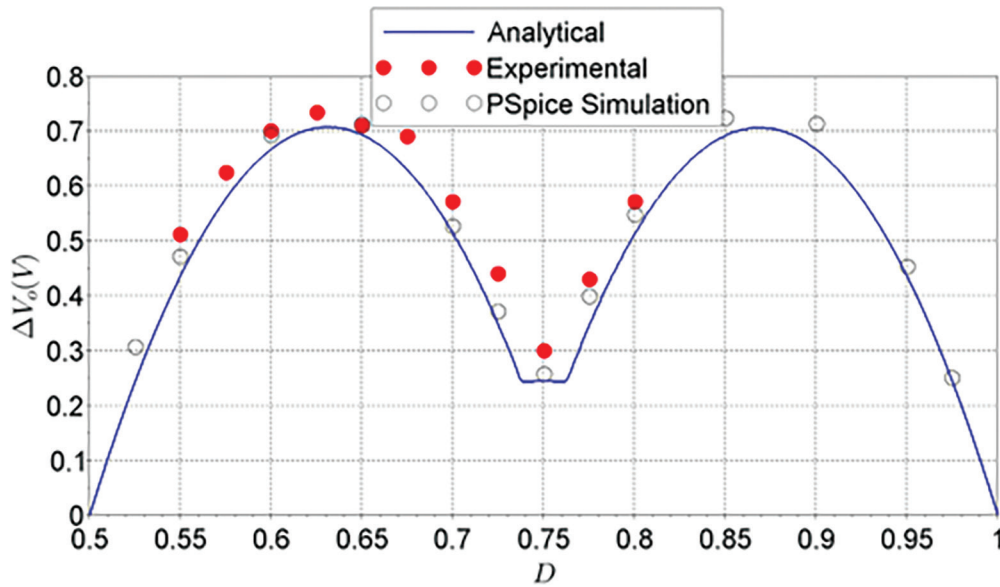


Fig. 28. Variation of ΔV_o as a function of D for TQPCs in series in phase-staggering mode operating at $\Phi = \Phi_{opt}$ obtained from analysis, experimental results and PSpice simulation under unequal input DC voltages. TQPCs, two-quadrant power converters.

It may be noted that the analytical and simulation results are obtained under the assumption that the filter component values in the two TQPCs are equal. In practice, it is very difficult to obtain perfectly matching components. Thus, with regard to the experimental prototype, it may be stated that the values of these components are slightly different, which can be attributed to the observed difference between experimental and analytical/simulation results.

6. Conclusion

In the context of series-connected TQPCs, the equation for output voltage of an individual TQPC is derived. It was verified that reduction in the ripple voltage in the overall output and increment in the ripple frequency occur with series-connected TQPCs operating in phase-staggering mode. Variation of ΔV_o as a function of F for 2-, 3-, 4-series-connected TQPCs is studied. This exercise suggested that ΔV_o is minimum for specific optimum phase shift Φ_{opt} . Variation of ΔV_o as a function of D for 2-, 3-, 4-series-connected TQPCs is studied in phase-staggering mode with optimum phase shift Φ_{opt} . These results are extrapolated for n -series-connected TQPCs to obtain expressions for Φ_{opt} and duty cycles for which minima and maxima of ΔV_o occur. Further, analysis is performed for two series-connected TQPCs in order to quantify the effect of various non-ideal conditions such as filter component tolerances, unequal input DC voltage of TQPCs, unequal duty cycles, and unequal on-state voltage drops in semiconductor devices. It was observed from analytical studies that the effect of unequal duty cycles and unequal on-state voltage drops in semiconductor devices on ΔV_o is not significant and thus can be neglected. The results of simulation studies for tolerance in filter component values and unequal input DC voltages were seen to be in good agreement with the analytical predictions. Further, experimental results on two prototypes, connected in series and fed with equal and unequal DC voltages, experimentally confirmed the analysis.

With the presented analysis, estimation of output voltage ripple was carried out in two series-connected TQPCs, and these estimations were performed under ideal as well as non-ideal conditions. The same methodology can be extended for a greater number of TQPCs connected in series. Using the predictions made by the presented analysis, the design of filter can be optimised, which in turn has a profound effect on the dynamics of the power converter and therefore the feedback control-loop design.

References

- Barbalat, O. (1992). Applications of particle accelerators. *CAE-CERN Accelerator School: 5th General Accelerator Physics Course*, Jyvaskyla, Finland, 7–18 September 1992.
- Bouteille, J. (2014). Power converters for cycling machines. In: *Proceedings CAS-CERN Accelerator School: Power Converters*, Baden, Switzerland, 7 – 14 May 2014.
- Burnet, J. (2014). Power converter requirements. In: *Proceedings CAS-CERN Accelerator School: Power Converters*, Baden, Switzerland, 7 – 14 May 2014.
- Chao, A. and Chou, W. (2011). Reviews of Accelerator Science and Technology. *World Scientific Publishing Company, Singapore*, 4, pp. v–vi (Editorial preface).
- Gros, P., Bobault, S. and Loulergue, A. (2006). The 3Hz power supplies of the SOLEIL. In: *Proceedings of EPAC 2006*, Edinburgh, Scotland, 26 – 30 June 2006.
- Kamaria, P. (2011). *Analytical and Experimental Studies on Various Electronics Subsystems Used in a Magnet Power Supply*. M.Tech. dissertation. Department of Electronics & Instrumentation Institute of Engineering and Technology Devi Ahilya Vishwavidyalaya, Indore.
- Marks, N., Griffiths, S., Theed, J.(2002). Configuration of the dipole magnet power supplies for the Diamond booster synchrotron. In: *Proceedings of EPAC 2002*, Paris, France, 3 – 7 June 2002.
- Pont, M., Petrocelli, R., Alloza, D., Yépez, D., Camell, R., Gross, G. and Burnet, J. (2010). Power converters for ALBA booster. In: *Proceedings of IPAC'10*, Kyoto, Japan, 23 – 28 May 2010.
- Rodrigues, C., Brunheira, G., Limeira, B. and Rogatto, G. (2019). Design and experimental results of a 1.1KA/800V AC power supply for Sirius booster dipoles. In: *10th International Particle Accelerator Conference (IPAC2019)*, Melbourne, Australia, 19–24 May 2019. <https://doi.org/10.18429/JACoW-IPAC2019-TUPMP001>.
- Semikron “SPT IGBT Module” SKM200GB128D datasheet [Online], (2006, September 11). Available at: <http://www.bjrted.com/pdf/skm200gb128d.pdf>
- Shi, J., Luo, J. and He, X. (2011). Common-Duty-Ratio Control of Input-Series Output-Parallel Connected Phase-shift Full-Bridge DC–DC Converter Modules. *IEEE Transactions on Power Electronics*, 11(26), pp. 3318–3329.
- Shimogawa, T., Kurimoto, Y., Morita, Y., Miura, K. and Naito, D. (2019). New power supply of main magnets for J-PARC main ring upgrade. In: *10th International Particle Accelerator Conference (IPAC2019)*, Melbourne, Australia, 19–24 May 2019. <https://doi.org/10.18429/JACoW-IPAC2019-TUPMP016>.
- Srivastava, A. (2022). *Analysis, Design and Development of Fast-Ramped, Switch-Mode Power Converter for Inductive Load*. M.Tech. dissertation. Homi Bhabha National Institute.
- Srivastava, A., Borage, M., Singh, A. and Dwivedi, V. (2023). Estimation of Control Loop Bandwidth for Desired Tracking Accuracy in a Fast-Ramped Power Converter for Electromagnets in Particle Accelerators. *International Journal of Power Electronics (In press)*.
- Srivastava, A., Borage, M., Singh, A., Dwivedi, V. and Tiwari, S. (2021). Steady-state analysis and design of two-quadrant, switch-mode, fast-ramped power converter for electromagnets in particle accelerators. In: *National Power Electronics Conference*, Bhubaneswar, India, 15–17 December 2021.
- Visintini, R. (2014). Power converters for accelerators. In: *Proceedings of the CAS-CERN Accelerator School: Power Converters*, Elettra Sincrotrone Trieste, Trieste, Italy, 7–14 May 2014.
- Visintini, R., Cautero, G., Cautero, M., Molaro, D., Svandriik, M. and Zaccaria, M. (2008). Magnet power converters for the new ELETTRA full energy injector. In: *Proceedings of EPAC08*, Genoa, Italy, 23–27 June 2008.
- Yang, X., Zong, S. and Fan, G. (2017). Analysis and validation of the output current ripple in interleaved buck converter. In: *IECON – 43rd Annual Conference of the IEEE Industrial Electronics Society*, Beijing, China, 29 October – 1 November 2017.